

Article

Stability Analysis of Strongly Weathered Muddy Slate Slopes Considering Softening Conditions of Water Immersion

Yungang Shi ¹, Jingyu Wang ², Xin Tan ^{3,*} , Suhua Zhou ³ , Yuxuan Jin ¹ and Xin Yin ³

¹ Hunan Communications Research Institute Co., Ltd., Changsha 410015, China; shiyungang1217@163.com (Y.S.)

² CCCC Construction Group Co., Ltd., Beijing 100022, China

³ College of Civil Engineering, Hunan University, Changsha 410082, China

* Correspondence: xintan@hnu.edu.cn; Tel.: +86-15-580-373-653

Abstract: To understand the stability of strongly weathered muddy slate slopes under water immersion effects, we obtained shear strength parameters of the weakly layered structures within this slate through direct shear tests. Point load tests were performed on in-site slate samples with varying water immersion durations to assess the water immersion's softening impact on slate strength. Results highlight that muddy slate strength presents pronounced random variability, declining as water immersion duration increases. Drawing from shear strength parameters and the water immersion softening observed in laboratory and in-site tests, we formulated a numerical slope model that considers layered structures and water immersion conditions to evaluate slope stability. Numerical simulations suggest that the slate slope's sliding surface, when layered, does not consistently form a basic circular arc or straight line. The slope safety factor (FOS) drops below 3, marking a notable decrease compared to a homogeneous slope (FOS = 3.22). In the model, multiple secondary sliding surfaces can emerge, leading to a sliding band with a specific thickness after introducing the random distribution of layer strength parameters. This further reduces the slope's FOS to below 2.9. Water immersion makes slopes inclined to slide following the layered structure. If the dip angle of the slate's layered structure is less steep than the slope's dip angle, water immersion notably diminishes the FOS, which can dip to a minimum of 1.12.



check for updates

Citation: Shi, Y.; Wang, J.; Tan, X.; Zhou, S.; Jin, Y.; Yin, X. Stability Analysis of Strongly Weathered Muddy Slate Slopes Considering Softening Conditions of Water Immersion. *Sustainability* **2023**, *15*, 14740. <https://doi.org/10.3390/su152014740>

Academic Editor: Jianjun Ma

Received: 2 September 2023

Revised: 29 September 2023

Accepted: 6 October 2023

Published: 11 October 2023



Copyright: © 2023 by the authors. Licensee MDPI, Basel, Switzerland. This article is an open access article distributed under the terms and conditions of the Creative Commons Attribution (CC BY) license (<https://creativecommons.org/licenses/by/4.0/>).

Keywords: muddy slate; water induced softening; bedding slope; lamination; slope stability

1. Introduction

The rock mass of natural rock slopes contains many discontinuous structural surfaces [1,2]. Numerous structural surfaces disrupt the continuity and integrity of the rock mass, giving it a strong anisotropic characteristic [3]. With the development of transportation project construction, many rock body slopes have emerged along these projects. Among them, with their natural layered structure, the strongly weathered bedding slate slopes are prone to destabilization accidents under extreme climatic conditions such as heavy rainfall and water inundation. This results in significant safety hazards and economic losses [4,5]. The shear strength parameter of the structural or laminar surface plays a significant role in controlling the stability of strongly weathered bedding slate slopes [6]. The softening of surfaces through water immersion can further diminish the rock mass's strength [7], leading to increased slope instability. Therefore, the stability of strongly weathered bedding slate slopes under inundation and softening conditions has garnered increasing attention. The mechanism behind its instability and destabilization has also become an urgent scientific research and engineering topic to be addressed. This has implications for the sustainability of infrastructure development.

The methods for determining the shear strength parameters of the structural face of the rock body mainly include laboratory and in-site tests [8–10]. The main methods are

laboratory and in-site tests, empirical formula estimation, numerical modeling [11], back calculation of measured displacements of slopes [12], and so on. Fan et al. [13] developed a model to represent bedding and counter-tilt slopes with discontinuous joints. They then investigated the dynamic response of these slopes using shaking table tests. This research contributes to the methods used to determine the shear strength parameters of rock faces. Dong et al. [14] used the layered mechanical parameters from the Brazilian disk splitting test to investigate the relationship between slate slope stability and damage mode and their bedding angles. Jiang et al. [15] developed a numerical model to assess the stability of bedding rock slopes. This model seamlessly integrates the Discrete Element Method (DEM) with a probability distribution model for joints and the softening characteristics exhibited by rock layers. Through this innovative approach, the researchers conducted a comprehensive analysis of layered slope stability, considering various working conditions. Furthermore, they scrutinized the forces acting upon the supporting structures associated with these slopes. Zhou et al. [16] conducted a study on the statistical attributes of shear strength concerning strongly weathered slate. They accomplished this through direct shear testing. In addition, they developed a numerical model to analyze bedding slopes. Their findings highlight the influence of two main factors: the variability of the dip angle of the bedding slope and the strength parameter. Notably, these factors collectively impact the slope's destabilization pattern and overall stability.

The research on water softening of slate is mainly focused on laboratory and in-site experiments [17] and microscopic interpretation of the water–rock interaction mechanism [18–20]. Among them, some studies focus on the effect of water level change on the mechanical properties of slopes [21–23]. Sun et al. [24], using the water-rich conditions of a coal mine as their engineering backdrop, conducted a series of tests. These included the uniaxial compression test, the conventional triaxial compression test, and the constant axial pressure test on cementitious sandstone. Concurrently, they established a multi-linear strain softening constitutive model. Wang et al. [25], Nian et al. [26], and Huang et al. [27] individually investigated the deterioration mechanism of slate upon contact with water. They approached this issue from both micro-mechanical and macro-mechanical perspectives, delving into the intricate details of the material's response. Liu et al. [28] utilized their independently developed multifunctional open-channel hydraulic test equipment. In conjunction with numerical simulation analysis, they explored the chemical, physical, and mechanical impacts of various flow patterns on the softening of red sandstone. Their research further unveiled the mechanisms behind how different flow patterns influence the softening of this material. Yang et al. [29] examined the alterations in strength within rock slopes that include weak layers while also analyzing the stability of these slopes in the context of heavy rainfall conditions. Li et al. [30] conducted drying and weathering tests, explicitly controlling the water content of the carbonaceous slate, and investigated the impact of water–rock interactions on the test specimens.

In this work, we focus on studying the characteristics of strength degradation in a strongly weathered muddy slate layer under water immersion conditions. Our study involves both laboratory and in-site experiments. We aim to establish a numerical slope model that accurately depicts the bedding angle of the layered structure in slate rock, the random strength distribution of weak layers, and the softening law of water immersion. The development of slope models will rely on our understanding of the strength rule, specifically acquired through our experiments on the weak layered structures of strongly weathered slate. Moreover, a series of numerical analyses have been conducted to help us understand the rules governing the slope stability changes of the strongly weathered slate with very typical anisotropic structures under various water immersion conditions. In addition, these analyses will assist in identifying the instability characteristics of such slopes.

2. Laboratory and In-Site Tests

Strongly weathered muddy slate specimens were taken from the slope surface exposed due to excavation on the Xialong Expressway in Guizhou Province, China. The layered

structure in the slate specimens of the slope body was well developed (Figure 1). Drill holes revealed the stratum distribution of the slope as follows: a surface thickness of 0.5–1.5 m for the Quaternary residual slope deposits of silty clay; the lower layer is a strongly weathered muddy slate with a thickness of 10–13 m, with a metamorphic layer structure, and developed cracks, along with a smooth cleavage surface. Below this is a moderately weathered muddy slate. As determined by the geological compass, the rock layer attitude of the slate slope at the site is inclination 120° , dip angle 34° . The strength of weak layers in a strongly weathered slate determines the slope stability; therefore, the direct shear and in-site point load tests were carried out after collecting specimens of strongly weathered slate containing weak layers from the field slope. The strongly weathered muddy slate exhibits significant weathering from the in-site slope excavation surface. Within the fractures, distinct brown staining is evident, but the overall cohesion is relatively good, and the extent of opening is not substantial.

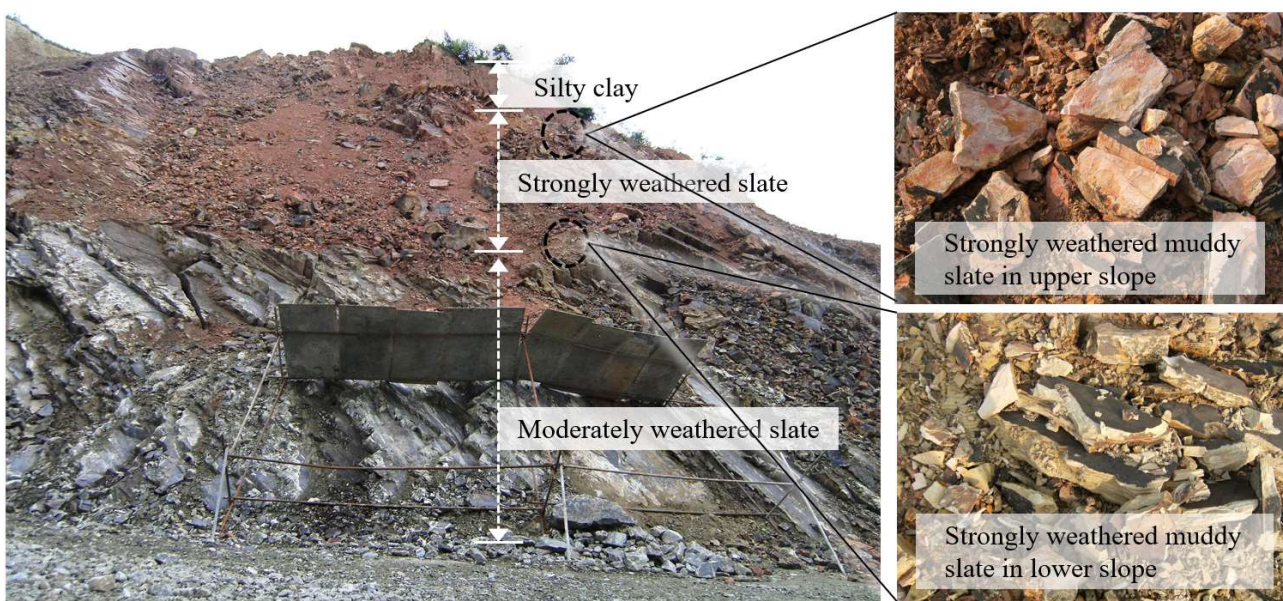


Figure 1. In-site slope location and rock photographs.

2.1. Direct Shear Test

The direct shear test was conducted using a self-designed loading device, illustrated in Figure 2. The tests adhered to the standards outlined in reference [31]. Given the low strength of the strongly weathered muddy slate, shaping it into a standard form to fit the device was challenging. Consequently, cement mortar mold casting was employed to produce the necessary specimens for the direct shear test. The weight ratio for the mortar mix was: cement: standard sand: water = 600 g: 1800 g: 240 g. Initially, the slate mass was shaped into a cube with 100 mm sides using a rock-cutting chainsaw. This ensured the shear surface of the specimen was no smaller than 70×70 mm. Half of a steel mold was filled with the cement mortar, into which the shaped specimen was pressed. This arrangement ensured the intended shear surface was aligned parallel to the opening of the steel mold, before the remaining cement mortar was added. After one day, the specimen was flipped onto the second half of the mold for compaction, ensuring the cement mortar fully enveloped the slate. Both steel mold halves were precisely aligned. The specimens were then stored at a room temperature of approximately 20°C to preserve humidity, with a curing period of at least 14 days.

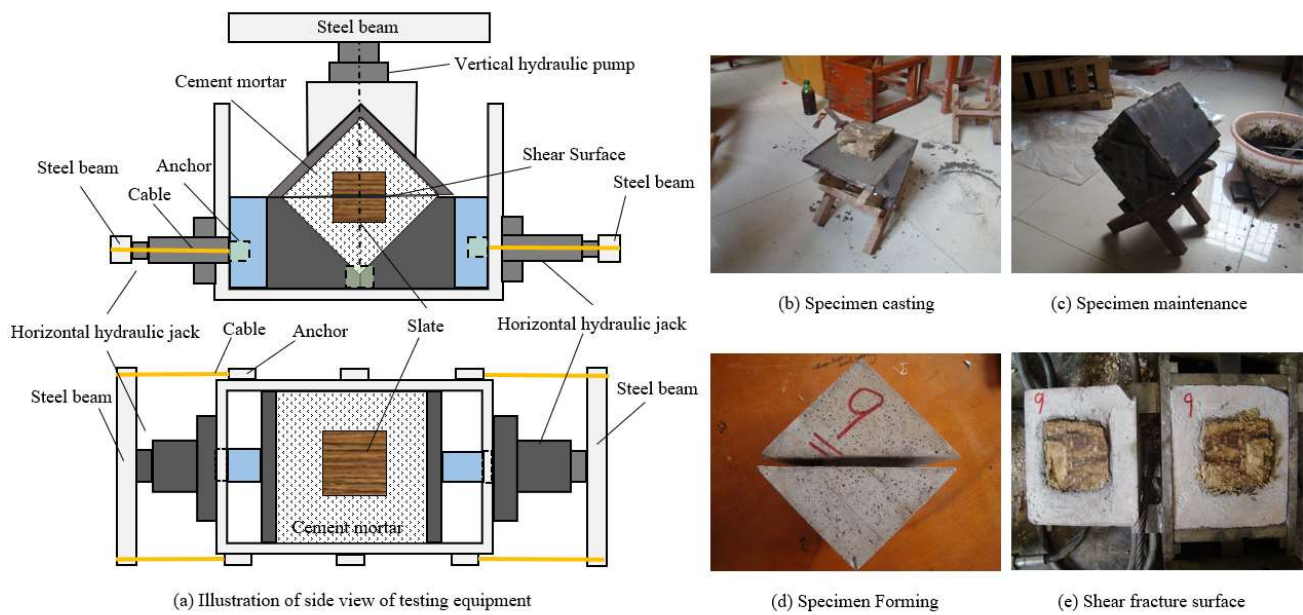


Figure 2. Direct shear device and preparation of direct shear specimens.

A total of twenty specimens were fabricated and subjected to direct shear tests using the following procedure: (1) Position the cured specimens centrally within the direct shear test device. (2) Use a vertical hydraulic pump to apply a normal force to the specimen in increments of 10% of the maximum designed normal force, noting the normal displacement at each stage. (3) Administer the shear force using horizontal hydraulic pumps in increments of 10% of the maximum designed shear force. Record the shear displacement at each stage. The loading process concludes once the residual strength is achieved. (4) Upon completing the loading phase, reduce the shear force first, followed by the normal force. Both forces should be decreased stepwise at 10% of their maximum values. (5) Examine the marks on the shear failure surface, capture photographs, document the shear surface friction, and measure the actual dimensions of the specimen's shear surface.

The strongly weathered muddy slate sourced from the slope site is characterized by a soil-yellow color, significant softening, and low rock strength. The boundaries between the weak layers are clearly defined. The shear surfaces are uneven with noticeable undulations, and scratch marks are visible on them. During shearing, some protrusions, especially at the edges of the specimens, are cut, causing the rocks to fragment under the combined compressive and shear forces. The shear stress and shear displacement curve derived from the direct shear test are illustrated in Figure 3a. Before reaching the peak shear strength, shear stresses under varied normal pressures rose with increasing shear displacement. The rate of this rise (shear stiffness) varies considerably, highlighting the inconsistent mechanical properties of the natural rock specimens. After reaching peak shear strength, different specimens demonstrated varying shear displacements before strength reduction. The peak shear strength values of specimens under diverse normal stress conditions are shown in Figure 3b. The Mohr–Coulomb shear strength parameters for the weak layers of the strongly weathered muddy slate were deduced through optimal linear fitting, resulting in $c = 95.85$ kPa and $\phi = 33.87^\circ$. As with shear stiffness, a significant random variability is evident.

2.2. Point Load Tests on Slate Specimens under Different Immersion Conditions

The cracks and pores between the muddy slate layers serve as primary channels for water to seep into the rock. In the weak layers, minerals and cement expand when soaked in water. Yet, the rock's internal sections undergo minimal changes due to their lower permeability, restricting water infiltration. Therefore, under extended water immersion, the pores and cracks in the weak layers of the strongly weathered muddy slate expand, resulting

in a weaker bond between particles. With increased immersion time, the cementitious materials in these layers dissolve and erode, leading to the loss of the surrounding cement. This brings the mineral particle surfaces into direct contact with water, triggering physical and chemical reactions that augment the softening process. At a macroscopic level, this appears as an ongoing reduction of shear strength in the weak layers, epitomizing the water-induced softening effect within the layered structures.

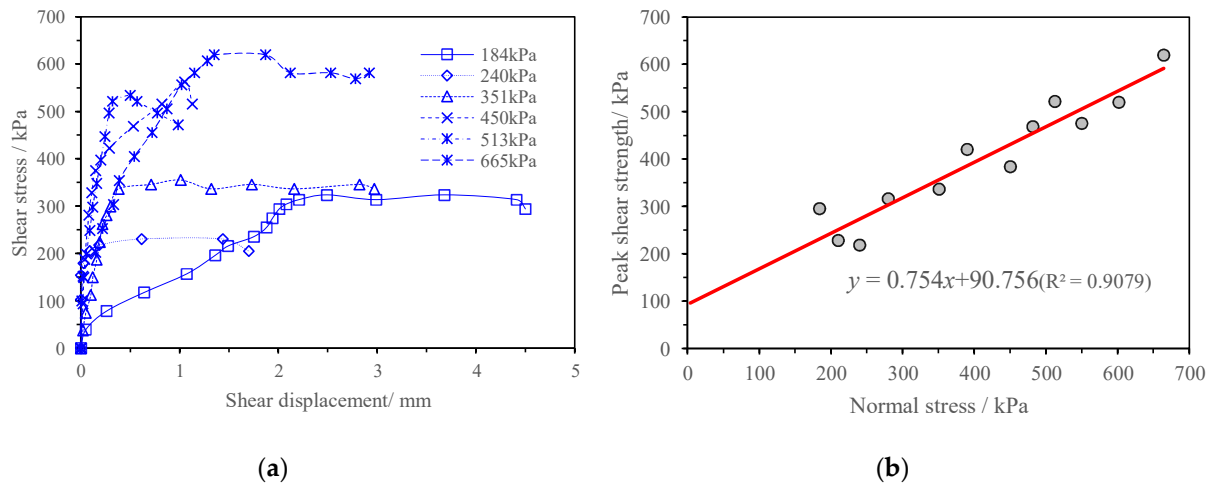


Figure 3. Results from direct shear tests: (a) direct shear test results; (b) fitted curve of weak layers' shear strength.

Given the constraints of time and budget, conducting numerous direct shear tests under various water immersion conditions is unfeasible. As a solution, we executed a series of point load tests on natural slate blocks from the slope field, each submerged for different durations. This helped depict the softening trend of the shear strength in weak layers of strongly weathered muddy slates under water immersion by establishing the relationship between point load strength and immersion duration. Point load testing is a swift rock mechanical assessment commonly done in the field. It gauges the mechanical strength of rocks under a point force and provides insights into the rock's quality, stiffness, and other attributes. For these tests, intact slate blocks were chosen from the slope field and were minimally processed to fit the specifications of the point load apparatus. Figure 4a displays the point load test set-up. Here, the slate specimen is positioned between a pair of conical loaders. The specimen's point load strength is determined by applying concentrated force through these loaders until the specimen fractures. When positioning the slate blocks, the parallel layer direction of the strongly weathered muddy slate was aligned as the loading direction. This alignment ensured that the resultant point load strength mirrored the inherent strength traits of the slate's weak layers. Before conducting the point load tests, the slate samples were soaked at the slope site for varying durations. Figure 4b presents the fractured specimens, all of which distinctly exhibit splitting along their weak layers.

The relationship between point load strength and water immersion duration is depicted in Figure 5. While the point load strength of slate blocks is not directly applicable for slope stability analysis, this relationship aids in understanding the softening law of the weak layer's shear strength in the slate specimens under study. We selected the average point load strength of the slate blocks in their natural state as the reference strength. The softening coefficient is defined as the ratio of the point load strength of slate blocks at various immersion durations to this reference strength. This coefficient encapsulates the impact of water immersion on the slate block's strength and, by extension, the strength of its weak layers. The results from the point load tests display notable variability; therefore, the softening coefficient curve was derived from a fitting based on all test outcomes. As Figure 5 indicates, an increase in immersion days leads to a steady decline in weak layer

strength. The fitting curve, depicting the softening coefficient as a function of immersion days, exhibits a negative exponential trend.

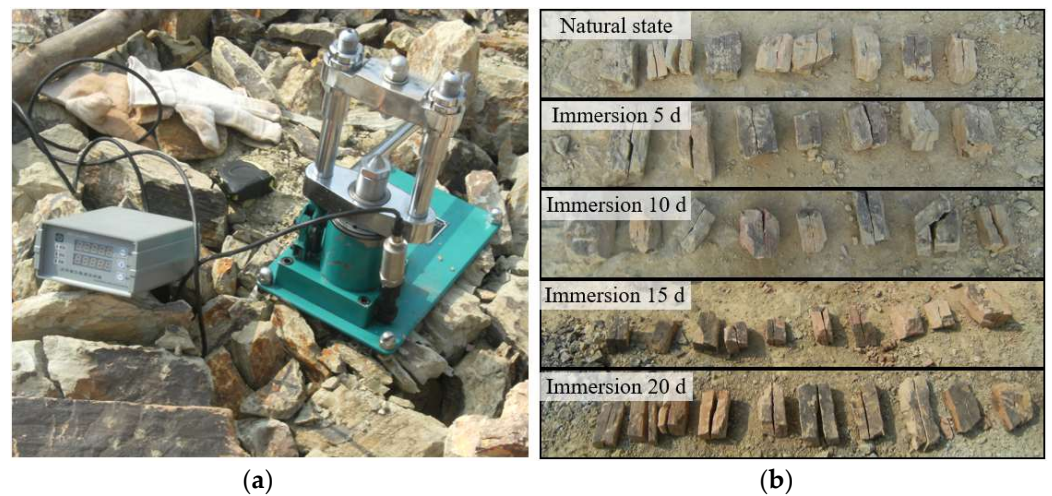


Figure 4. Point load tests: (a) point load test device; (b) fractured slate specimens.

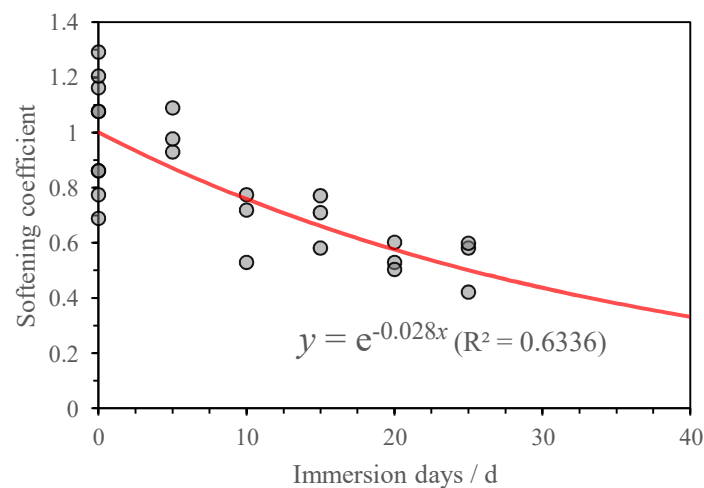


Figure 5. Relationship between immersion days and softening coefficient.

3. Numerical Model

The laboratory and in-site tests detailed in the previous section highlight several crucial factors for the stability analysis of the strongly weathered muddy slate slope: the dip angle of the slate bedding, shear strength parameters of the weak layers in strongly weathered muddy slate, spatial variability, and the water immersion softening law. In light of these factors, we established a numerical model of the layered slate slope using the FLAC3D program, illustrated in Figure 6. The slope body utilizes the Ubiquitous-Joint constitutive model. This model extends the Mohr–Coulomb constitutive model by incorporating additional shear strength and tensile strength parameters for weak planes. Consequently, it accommodates the potential for failure in both intact rock and weak layers. As such, the numerical slope model can represent rock failure, bedding plane failure, or a combined failure of both. This outcome chiefly depends on the slope element's stress state, the dip angle of the bedding planes, and the relative mechanical strength between the intact rock and the weak layers.

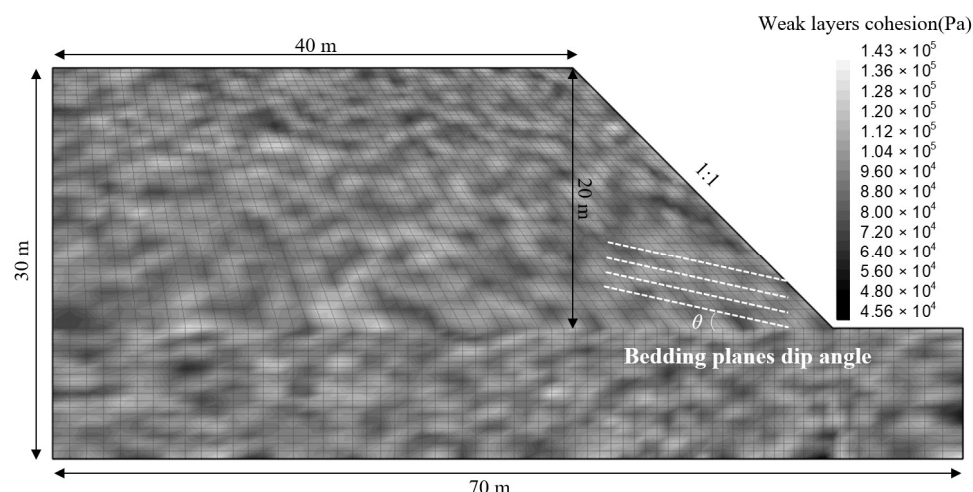


Figure 6. Numerical model considering spatial variability of shear strength of weak layers.

Both laboratory and in-site test results highlighted significant variability in strength parameters. Additionally, a wealth of existing research suggests that the normal distribution function effectively captures the statistical distribution of geotechnical strength parameters [32]. Thus, in our numerical model, we employed a normal distribution to dictate the spatial random variability of weak layer shear strength parameters. Assuming the friction angle, cohesion, and tensile strength of weak layers in the model are independent variables, the strength parameters for the model's elements were set to adhere to a random normal distribution, consistent with experimental findings. For instance, Figure 6 displays the spatial random distribution of weak layer cohesions within the slope model. Table 1 provides the means and standard deviations for each model parameter.

Table 1. Numerical model parameter table.

Parameters	Friction Angle ($^{\circ}$)		Cohesion (kPa)		Tensile Strength (kPa)		Elastic Modulus (MPa)	Poisson's Ratio
	Average Value	Standard Deviation	Average Value	Standard Deviation	Average Value	Standard Deviation		
Rock	38	5	200	20	100	5	800	0.35
Weaklayer	33	5	100	20	30	5	/	/

Figure 6 displays the dimensions of the numerical model, where all boundaries are simply supported except for the slope surface. Once the numerical model achieved initial equilibrium under gravity, the strength reduction method was applied for slope stability analysis. The strength parameters of the slope, encompassing both the intact rock and weak layers, were systematically reduced until the model approached a critical instability threshold, determining the safety coefficient. Concurrently, based on the shear strain rate distribution within the numerical models, the position and contour of the sliding surface at the point of slope instability were identified.

4. Numerical Analysis Results and Discussion

4.1. Influence on Slope Stability from Weak Layered Structures

Figure 7 presents the slope stability analysis results for models with and without weak layered structures, detailing both the safety factor and the shear strain rate distribution. The concentrated shear strain rate, represented by the red band in Figure 7, can be interpreted as the sliding surface during slope instability. In the homogeneous model, without weak layered structures, the safety factor stands at 3.22, and the sliding surface resembles an arc segment passing through the slope's base (Figure 7a). In models that account for weak layered structures, the sliding surface is distinctly influenced by these structures, and

this influence varies based on the bedding dip angle. For a gentle bedding dip angle, as demonstrated in Figure 7b ($\theta = 10^\circ$), the upper part of the sliding surface aligns with that of the homogeneous slope. This suggests that the upper part of a gently dip bedding slope's stability is predominantly determined by the intact rock's strength. The slope's lower segment, however, is notably influenced by the bedding planes, adhering to the bedding dip direction. Given the stress concentration at the slope's toe, weak layers are more likely, promoting sliding along the bedding. As the bedding dip angle sharpens, evident in Figure 7c ($\theta = 40^\circ$), the gravitational force pulling the slide along the bedding dip direction intensifies, making along-bedding slides more probable. Consequently, the sliding surface's shape largely conforms to the bedding dip direction, with the slope's stability primarily dictated by the weak layer's strength. In scenarios with even steeper bedding dip angles, as seen in Figure 7d ($\theta = 60^\circ$), the sliding surface largely mirrors that of the homogeneous slope. With diminished sliding forces on steeply dipping beds, the slope is less susceptible to instability sliding in the direction of the bedding dip. Concerning the slope's safety factor, it is clear that a numerical slope model incorporating weak layered structures will possess a safety factor inferior to that of a homogeneous model. However, since the natural state's weak layer strength parameters are not drastically low, the safety factors of slope models under varying bedding dip angles do differ. Still, the overall discrepancies are not pronounced.

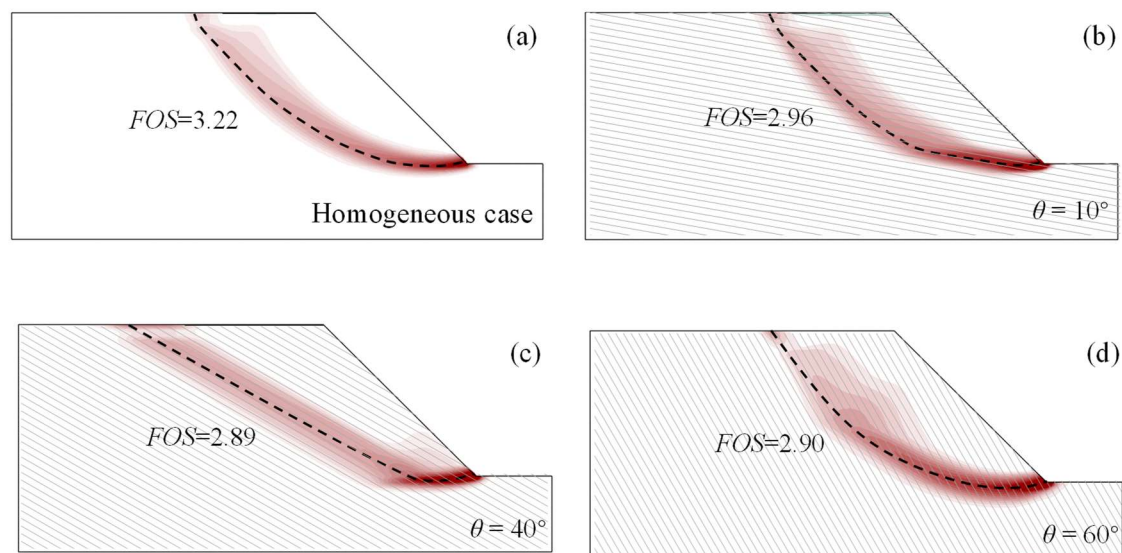


Figure 7. Slope stability analysis results with and without weak layered structures: (a) homogeneous case; (b) $\theta = 10^\circ$; (c) $\theta = 40^\circ$; (d) $\theta = 60^\circ$.

4.2. Influence on Slope Stability from Strength Spatial Stochastic Variability

Figure 8 contrasts the slope stability results between numerical models that factor in the spatial random variability of weak layer strength parameters and those that do not. While the model that incorporates spatial random variability exhibits a sliding surface shape akin to the model where weak layer strength parameters are constant, there are distinct differences. The constant parameter model portrays a sliding surface as a relatively smooth arc or linear form. In contrast, the model recognizing parameter random distribution may display several secondary sliding surfaces. These secondary sliding surfaces, combined with the primary sliding surface, create a noticeable thickness of a sliding band, diverging from the smooth sliding contour. The instability pattern in the model considering parameter random distribution more accurately mirrors the real-world conditions of natural slopes. By integrating the statistical distribution attributes of strength parameters, the model introduces regions of comparatively weaker strength parameters, often termed a “weak chain”. This inclusion invariably lowers the model's slope safety factor.

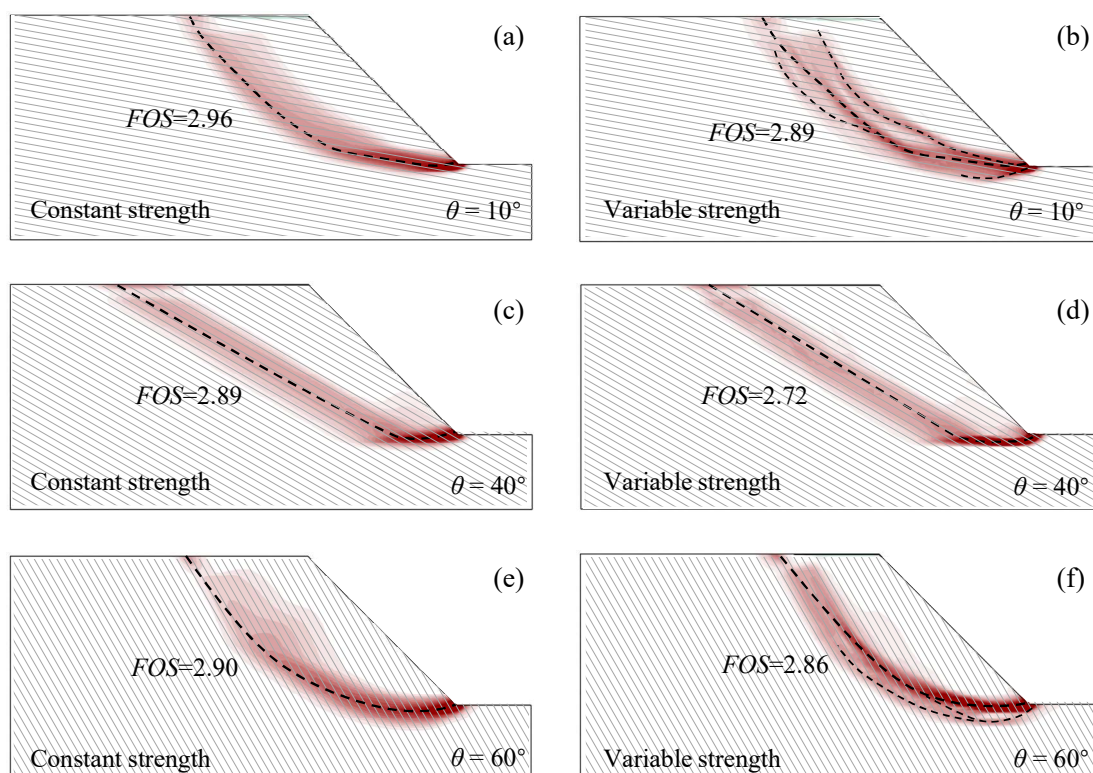


Figure 8. Slope stability analysis results with and without considerations of the strength spatial random variability: (a) constant strength, $\theta = 10^\circ$; (b) variable strength, $\theta = 10^\circ$; (c) constant strength, $\theta = 40^\circ$; (d) variable strength, $\theta = 40^\circ$; (e) constant strength, $\theta = 60^\circ$; (f) variable strength, $\theta = 60^\circ$.

Figure 9 consolidates the safety factors of all slope models in their natural state. The introduction of weak layered structures, coupled with the strength's spatial random variability, notably diminishes the slope safety factors. Across varied bedding dip angles, as the dip angle ascends from horizontal to around 50° , the sliding surface shape becomes increasingly dictated by the weak layers, leading to a consistent decrease in the safety factor. However, as the bedding dip angle steepens (from 50° to 80°), the safety factor begins to rise with the growing angle. When the bedding becomes vertical, the safety factor drops again, likely due to toppling failure caused by the vertical bedding orientation. The analysis results highlight that the most disadvantageous bedding dip angle for the strongly weathered muddy slate slopes is roughly 40° . Yet, given the natural state's weak layer shear strength of the strongly weathered muddy slate, the safety factor consistently remains above 2.7 for all bedding dip angle scenarios. This ensures the stability of natural slopes in the expressway construction area.

4.3. Influence on Slope Stability from Water Immersion Durations

Assuming that the weak layers' shear strength adheres to the water-induced softening law depicted in Figure 5, we used the softening reduction formula to determine the reduced cohesion and tensile strength of weak layers for various water immersion durations. This approach enabled us to use numerical models to investigate the effects of water-induced softening on slope stability. Figure 10 presents the stability analysis results for slopes with varied bedding dip angles after immersion in water for 5, 20, and 100 days.

For slopes with gentle-dip bedding, where the dip angle is less than the slope inclination (Figure 10a–f, $\theta = 20^\circ, 40^\circ$), extended water immersion periods lead to diminished weak layer strength. This makes the slope more susceptible to instability, typically resulting in sliding along a path that cuts through the weak layer towards the slope's face. Conversely, for steep-dip bedding slopes, where the bedding dip angle exceeds the slope inclination (Figure 10g–l, $\theta = 60^\circ, 80^\circ$), the existence of a free face prevents the formation of

a continuous sliding surface along a specific weak layer. As a result, the instability retains a similar arc-shaped pattern, but within certain regions of the sliding surface, particularly the upper section, it tends to follow the bedding direction.

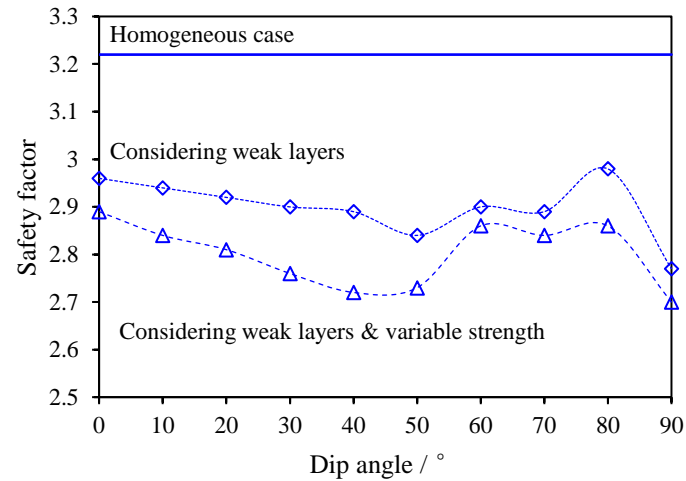


Figure 9. Comparison of safety factors of slope models under different conditions.

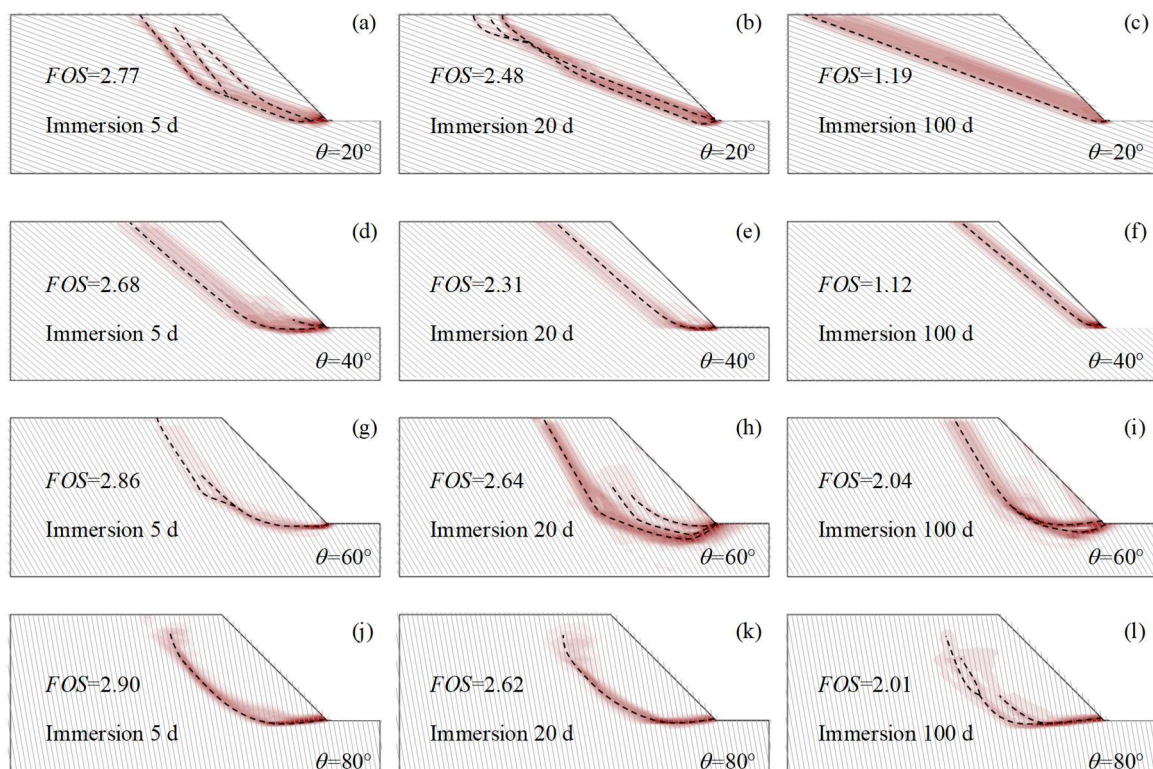


Figure 10. Numerical results of slopes with distributed shear strength parameters and different layer angles after water softening: (a) immersion for 5 days, $\theta = 10^\circ$; (b) immersion for 20 days, $\theta = 10^\circ$; (c) immersion for 100 days, $\theta = 10^\circ$; (d) immersion for 5 days, $\theta = 40^\circ$; (e) immersion for 20 days, $\theta = 40^\circ$; (f) immersion for 100 days, $\theta = 40^\circ$; (g) immersion for 5 days, $\theta = 60^\circ$; (h) immersion for 20 days, $\theta = 60^\circ$; (i) immersion for 100 days, $\theta = 60^\circ$; (j) immersion for 5 days, $\theta = 80^\circ$; (k) immersion for 20 days, $\theta = 80^\circ$; (l) immersion for 100 days, $\theta = 80^\circ$.

Figure 11 presents the slope safety factors derived from various water immersion durations and bedding dip angles, visualized as curves. These curves elucidate the relationships among slope safety factor, immersion duration, and bedding angle. Figure 11a highlights the change in slope safety factors relative to water immersion duration. As this

duration increases, the safety factors of the slope models, across various bedding dip angles, tend to decrease. This decline is most pronounced for angles between 20° and 40° . In Figure 11b, the interplay between slope safety factors and bedding dip angles is showcased. In their unaltered state, the strength parameters of the bedding are notably robust. While the bedding dip angles have some effect on the slope safety factors, their impact remains relatively muted. However, as the bedding strength diminishes with prolonged water immersion, the predominant mode of slope failure becomes increasingly aligned with the bedding planes. At this juncture, the bedding dip angles exert a more pronounced influence on the slope safety factors, especially in the 20° to 40° range. After 100 days of water immersion, the safety factors of slopes within this angle range dip below the standard engineering benchmark of 1.25 for expressway constructions, emphasizing the need for increased vigilance in engineering practices. Figure 12 further details the three-dimensional relationship connecting slope safety factors, immersion duration, and bedding dip angles.

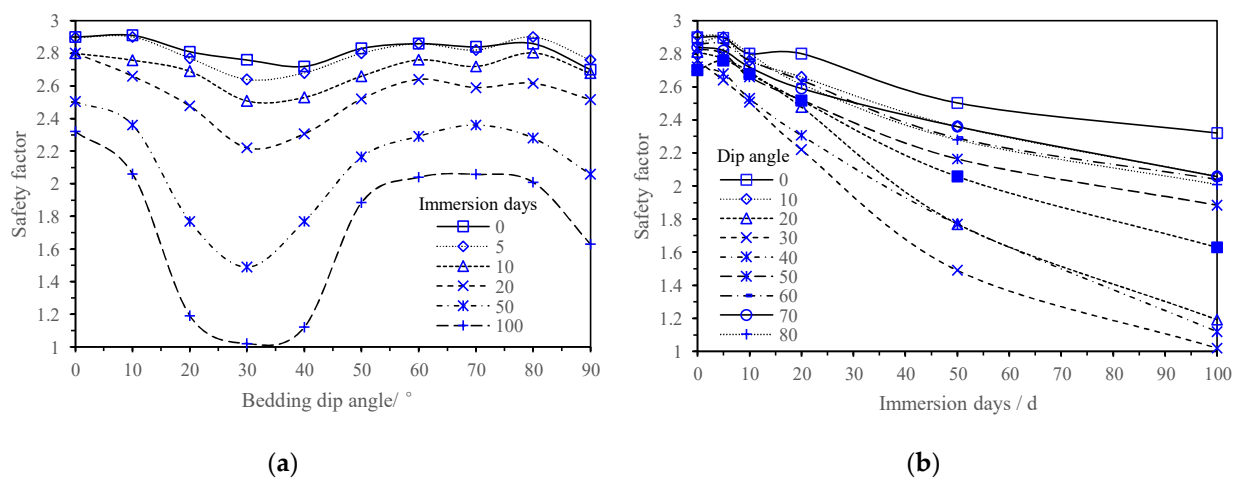


Figure 11. Comparison of safety factors of slope models under different bedding dip angles and water immersion durations: (a) the relationship between the slope safety factor and the number of days of inundation; (b) variation of slope safety factor as a function of bedding dip.

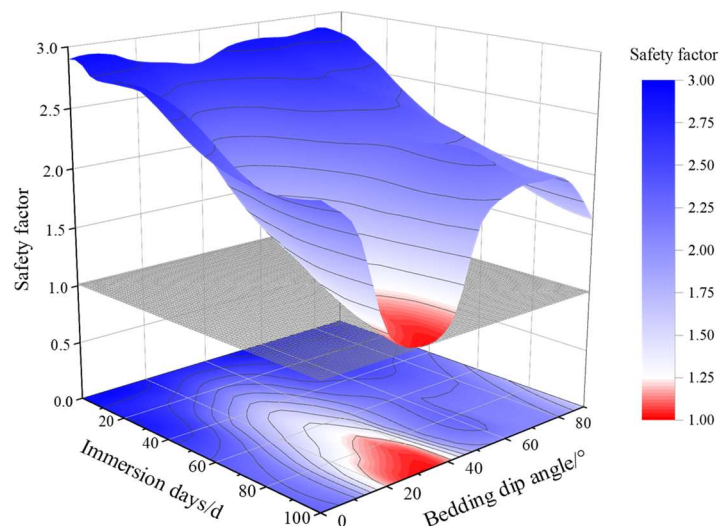


Figure 12. Three-dimensional relationship between slope safety factor, bedding dip angle, and immersion duration.

5. Conclusions

In this study, we introduced an innovative approach to understanding the destabilization of strongly weathered muddy slate slopes. Through direct shear tests using a

custom-designed device, we determined the shear strength parameters of the slate's weak layers. Additionally, point load tests under varying water immersion durations revealed the softening pattern of these weak layers. From these findings, we developed a unique numerical model for layered slate slopes, leading to several key insights:

1. Our model accurately captures the complexities of real-world slopes, including the weak layer's strength, slate bedding's dip angle, and the softening effects of water immersion. Notably, the model predicts instability patterns that reflect the multifaceted nature of natural slopes.
2. The model identifies areas of reduced strength, termed "weak chain" regions. These areas, arising from spatial parameter variations, significantly impact the slope's safety factor, highlighting the importance of accounting for such variations in slope stability assessments.
3. Water immersion plays a pivotal role in slope stability. As immersion progresses, the strength of the weak layers diminishes, making them a dominant factor in slope stability, especially in gently inclined slopes. This finding underscores the need for careful monitoring and consideration of slopes susceptible to water immersion.

In closing, while our study sheds light on the effects of complete submersion, it is vital to recognize that natural slopes often experience localized inundation. Future research should focus on these more common inundation scenarios.

Author Contributions: Conceptualization, Y.S.; investigation, J.W., S.Z. and Y.J.; supervision, X.T.; writing—review and editing, X.T.; visualization, X.Y.; software, X.Y. All authors have read and agreed to the published version of the manuscript.

Funding: This research was funded by "National Natural Science Foundation of China (52278348)", "Transportation Science and Technology Development and Innovation Project of Hunan Province (202303-2)" and "Science and Technology Infrastructure Program of Guizhou Province (2020-4Y047)".

Institutional Review Board Statement: Not applicable.

Informed Consent Statement: Not applicable.

Data Availability Statement: Not applicable.

Conflicts of Interest: The authors declare no conflict of interest.

References

1. Li, E.; Wei, Y.; Chen, Z.; Archbold, P.; Mullarney, B. Experimental Study on Tensile Characteristics of Layered Carbonaceous Slate Subject to Water–Rock Interaction and Weathering. *Sustainability* **2023**, *15*, 885. [\[CrossRef\]](#)
2. Tan, X.; Konietzky, H.; Frühwirt, T.; Dan, D.Q. Brazilian tests on transversely isotropic rocks: In-site testing and numerical simulations. *Rock Mech. Rock Eng.* **2015**, *48*, 1341–1351. [\[CrossRef\]](#)
3. Zhang, Z.; Cheng, Y.; Song, Z.; Ye, X. Anisotropy and Directivity Effects on Uniaxial Compression of Carbonaceous Slate Form Jinman Mine. *Appl. Sci.* **2022**, *12*, 9811. [\[CrossRef\]](#)
4. Song, Y.; Zheng, J.; Ma, H.; Shao, Z.; Yang, J.; Shen, F.; Liu, C. Study on Uniaxial Mechanical Behavior and Damage Evolution Mechanism of Water-Immersed Mudstone. *Sustainability* **2023**, *15*, 12499. [\[CrossRef\]](#)
5. Shan, Z.; Lv, J.; Zhang, F.; Chen, L.; Yin, F.; Dong, M. Different Toppling Bank Slope Failures under Hydrodynamic Action during Impoundment of the Miaowei Hydropower Station Reservoir. *Water* **2022**, *14*, 2126. [\[CrossRef\]](#)
6. Wang, Z.; Xia, Y.; Xia, G.; Jing-dong, L.; Dong, C. An experimental study of shear strength characteristics of structural plane of bedding rock slope. *Rock Soil Mech.* **2015**, *36*, 193–200.
7. Xu, X.; Zhou, Y.; Chen, W.; Gao, Y.; Fu, Q.; Liu, X.; Feng, C. Macro-Microscopic Deterioration Behavior of Gypsum Rock after Wetting and Its Constitutive Model Based on Acoustic Emission. *Minerals* **2022**, *12*, 1168. [\[CrossRef\]](#)
8. Sanei, M.; Faramarzi, L.; Fahimifar, A.; Goli, S.; Mehinrad, A.; Rahmati, A. Shear strength of discontinuities in sedimentary rock masses based on direct shear tests. *Int. J. Rock Mech. Min. Sci.* **2015**, *75*, 119–131. [\[CrossRef\]](#)
9. Luo, H.; Cheng, D.; Cheng, H.; Chong, J.; Zhao, C.; Ce, S.; Lin, L. Back analysis test on mechanical property and parameters of structure surface to direct shear in fracture rock mass. *J. Railw. Sci. Eng.* **2017**, *14*, 1886–1892.
10. Tan, X.; Ren, Y.K.; Li, T.L.; Zhou, S.H.; Zhang, J.C.; Zhou, S.K. In-situ direct shear test and numerical simulation of slate structural planes with thick muddy interlayer along bedding slope. *Int. J. Rock Mech. Min. Sci.* **2021**, *143*, 104791. [\[CrossRef\]](#)
11. Park, J.W.; Song, J.J. Numerical simulation of a direct shear test on a rock joint using a bonded-particle model. *Int. J. Rock Mech. Min. Sci.* **2009**, *46*, 1315–1328. [\[CrossRef\]](#)

12. Wu, M.; Liu, K. Study of inversion method for analyzing slope weight displacement and engineering application. *Ind. Constr.* **2015**, *45*, 122–125.
13. Fan, Y.; Zhang, W.; Zhou, Z. Research on dynamic response of rock slopes with discontinuous joints. *J. Railw. Sci. Eng.* **2017**, *14*, 1184–1191.
14. Dong, H.; Zhang, H.; Fu, H. Research on the bedding slate slope slip-crack destruction based on Brazilian disk splitting tests. *J. Railw. Sci. Eng.* **2014**, *11*, 94–100.
15. Jiang, H. Stability analysis of bedding rock shope reinforced by micro-piles and prestressed anchor. *J. Railw. Sci. Eng.* **2019**, *16*, 2184–2191.
16. Zhou, S.H.; Zhou, S.K.; Zhang, J.C.; Tan, X. Effect of bedding orientation and spatial variability of stratification shear strength on the stability of transversely isotropic rock slope. *Front. Phys.* **2021**, *9*, 777216. [[CrossRef](#)]
17. Sun, L.; Tang, X.; Abdelaziz, A.; Liu, Q.; Grasselli, G. Stability analysis of reservoir slopes under fluctuating water levels using the combined finite-discrete element method. *Acta Geotech.* **2023**, *18*, 5403–5426. [[CrossRef](#)]
18. Ping, S.; Wang, F.; Wang, D.; Li, S.; Yuan, Y.; Feng, G.; Shang, S. Multi-scale deterioration mechanism of shear strength of gypsum-bearing mudstone induced by water-rock reactions. *Eng. Geol.* **2023**, *323*, 107224.
19. Bian, K.; Liu, J.; Zhang, W.; Zheng, X.; Ni, S.; Liu, Z. Mechanical behavior and damage constitutive model of rock subjected to water-weakening effect and uniaxial loading. *Rock Mech. Rock Eng.* **2019**, *52*, 97–106. [[CrossRef](#)]
20. Hu, X.; Bian, K.; Liu, J.; Xie, Z.-Y.; Chen, M.; Li, B.-Y.; Cen, Y.; Liu, Z.-P. Discrete element simulation of shale softening based on parallel-bonded water-weakening model. *Chin. J. Geotech. Eng.* **2021**, *43*, 725–733.
21. Wu, Q.; Liu, Y.; Tang, H.; Kang, J.; Wang, L.; Li, C.; Wang, D.; Liu, Z. Experimental study of the influence of wetting and drying cycles on the strength of intact rock samples from a red stratum in the three Gorges Reservoir area. *Eng. Geol.* **2023**, *314*, 107013.
22. Fang, J.; Deng, H.; Li, J.; Xie, Z.-Y.; Chen, M.; Li, B.-Y.; Cen, Y.; Liu, Z.-P. Study on the seepage characteristics and degradation mechanism of a single-jointed sandstone under the cyclic dry–wet process in the three Gorges reservoir. *Bull. Eng. Geol. Environ.* **2021**, *80*, 8123–8136.
23. Xiao, J.; Li, Y.; Cai, J. Model test research on response characteristics of Outang landslide under water level fluctuation. *J. Eng. Geol.* **2020**, *28*, 1049–1056.
24. Sun, Z.; Wang, K.; Kang, Y.; Hu, W. A Study on the Strain-Softening Constitutive Model of Cementitious Sandstone. *Water* **2022**, *14*, 1309. [[CrossRef](#)]
25. Wang, L.; Li, T.; Zhang, J. study on the influence of groundwater on the microstructure of slate. *Water Power* **2019**, *45*, 45–48.
26. Nian, H.; Zhang, C. Study of micro-softening mechanism and strength mode of saturated slate in reservoir area of Wudongde hydropower station. *J. China Three Gorges Univ. Nat. Sci.* **2018**, *40*, 6–10.
27. Huang, Z.G.; Zuo, Q.J.; Wu, L.; Chen, F.B.; Hu, S.S.; Zhu, S. Nonlinear softening mechanism of argillaceous slate under water-rock interaction. *Rock Soil Mech.* **2020**, *41*, 2931–2942.
28. Liu, Z.; He, X.; Zhou, C. Influence Mechanism of Different Flow Patterns on the Softening of Red-Bed Soft Rock. *J. Mar. Sci. Eng.* **2019**, *7*, 155. [[CrossRef](#)]
29. Yang, Y.C.; Xing, H.G.; Yang, X.G.; Chen, M.L.; Zhou, J.W. Experimental study on the dynamic response and stability of bedding rock slopes with weak interlayers under heavy rainfall. *Environ. Earth Sci.* **2018**, *77*, 433. [[CrossRef](#)]
30. Li, E.; Feng, J.; Zhang, L.; Zhang, H.-C.; Zhu, T.-Y. Brazilian tests on layered carbonaceous slate under water-rock interaction and weathering. Brazilian tests on layered carbonaceous slate under water-rock interaction and weathering. *Chin. J. Geotech. Eng.* **2021**, *43*, 329–337.
31. *JTGE41-2005*; Test Methods of Rock for Highway Engineering. China Communications Press: Beijing, China, 2005.
32. Kong, L.; Li, C. Research on window width optimization and interval truncation for inferring probability distribution of geotechnical parameters by normal information diffusion method. *J. Railw. Sci. Eng.* **2021**, *18*, 2600–2609.

Disclaimer/Publisher’s Note: The statements, opinions and data contained in all publications are solely those of the individual author(s) and contributor(s) and not of MDPI and/or the editor(s). MDPI and/or the editor(s) disclaim responsibility for any injury to people or property resulting from any ideas, methods, instructions or products referred to in the content.